CHEMISTRY
A EUROPEAN JOURNAL

ChemPubSoc
Europe

DOI: 10.1002/chem.201201940

Unusual Salt-Induced Color Modulation through Aggregation-Induced Emission Switching of a Bis-cationic Phenylenedivinylene-Based π Hydrogelator

Santanu Bhattacharya*[a, b] and Suman K. Samanta[a]

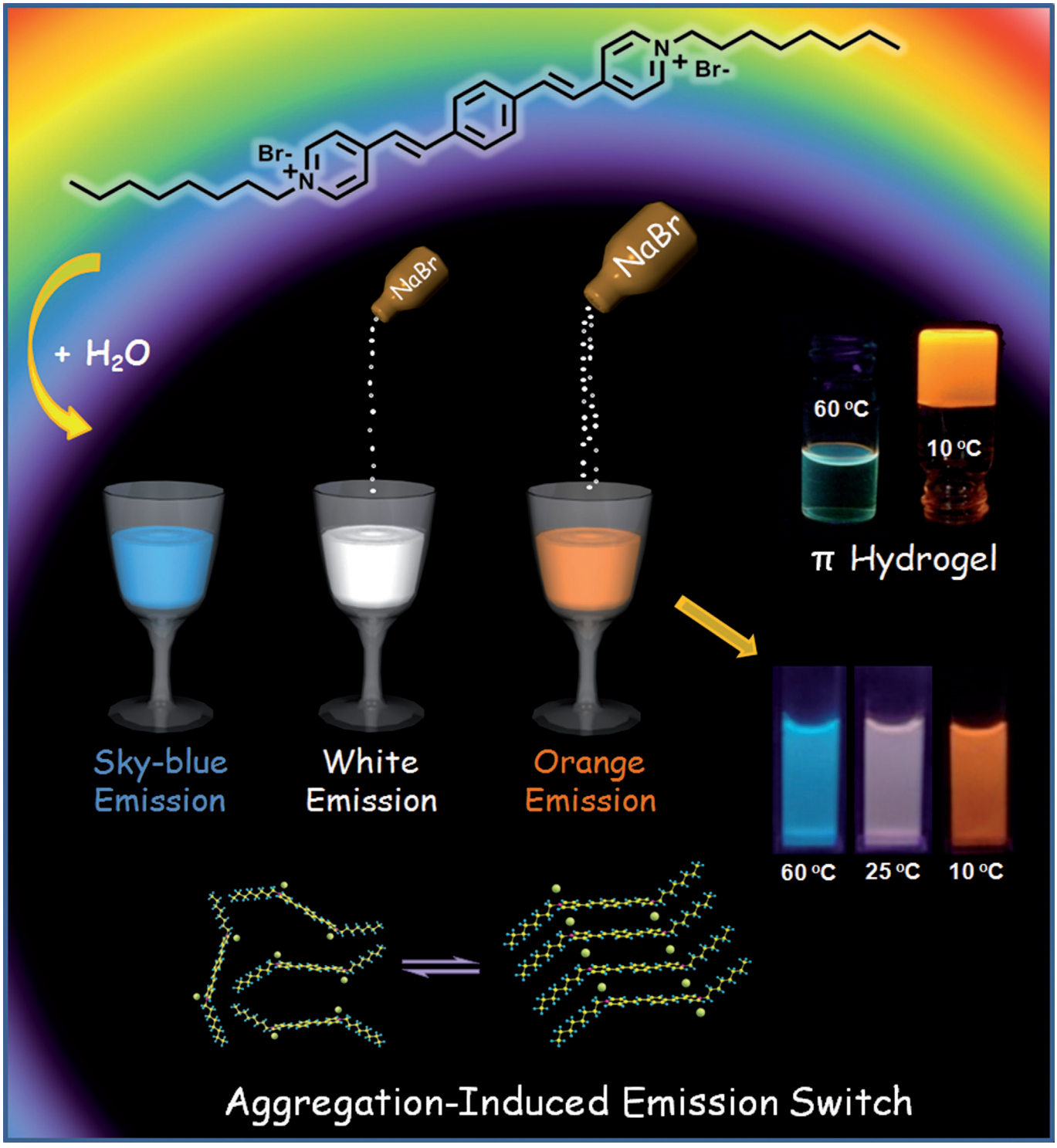

Abstract: The synthesis, hydrogelation, and aggregation-induced emission switching of the phenylenedivinylene bis-*N*-octyl pyridinium salt is described. Hydrogelation occurs as a consequence of π-stacking, van der Waals, and electrostatic interactions that lead to a high gel melting temperature and significant mechanical properties at a very low weight percentage of the gelator. A morphology transition from fiber-to-coil-to-tube was observed depending on the concentration of the gelator. Variation in the added salt type, salt concentrations, or temperature profoundly influenced the order of aggregation of the gelator molecules in aqueous solution. Formation of a novel chromophore assembly in this way leads to an aggregation-induced switch of the emission colors. The emission color switches from sky blue to white to orange depending upon the extent of aggregation through mere addition of external inorganic salts. Remarkably, the salt effect on the assembly of such cationic phenylenedivinylenes in water follow the behavior predicted from the well-known Hofmeister effects. Mechanistic insights for these aggregation processes were obtained through the counterion exchange studies. The aggregation-induced emission switching that leads to a room-temperature white-light emission from a single chromophore in a single solvent (water) is highly promising for optoelectronic applications.

Keywords: aggregation · chromophores · gels · salt effect · thermoreversibility

Introduction

Supramolecular association of low-molecular-mass gelators (LMMGs) gives rise to viscoelastic gels with attractive aggregation-induced properties.[1] These aggregates in the form of rods, fibers, tubules, coils, and so forth[2] provide a route for the generation of nano- or microsized soft materials for the fabrication of optoelectronic devices.[3] Self-assembly of photochromic gelators driven by noncovalent interactions leads to a chromophore assembly, which is often responsible for their impressive optoelectronic properties as well as their use in imaging and sensing applications.[4] Indeed, interesting photophysical properties have been recorded with oligo(*p*-phenylenevinylene)-based systems.[5] However, achieving control over the aggregation of the individual gelators to produce emission switches depending upon the extent of aggregation still remains a challenge. Also, most of the instances that involve supramolecular association of these conjugated chromophoric molecules are restricted to gel formation in organic media. Aqueous solubility of these conjugated molecules is important because the charged conjugated systems that involve oligo(*p*-phenylenevinylenes)[6] and oligo(*p*-phenyleneethyneylenes)[7] have received particular attention due to their antibacterial and antiviral activities. They are also potentially useful in imaging.

Herein, we report a novel π-hydrogel system based on the conjugated bis-pyridinium phenylenevinylene (PPV) moiety and its unique aggregation-induced emission switching properties. The emission color switches from sky blue to white to orange upon simple addition of different inorganic salts in varying concentrations in solution. Interestingly, the observed effects follow the well-known Hofmeister series, which offers a trend in the propensity of ions to induce the folding/unfolding of proteins and other macromolecules in aqueous media. To the best of our knowledge, such salt-induced control of aggregation of small molecules (e.g., LMMGs) and the remarkable effect on emission switching are hitherto unreported. Also, room-temperature white-light emission from a single chromophore in a single solvent (water) holds potential for optoelectronic applications and makes the system especially interesting for a detailed investigation.

Results and Discussion

Synthesis: The chromophoric phenylenedivinylene bis-pyridinium (PPV) gemini amphiphiles were synthesized by using a fixed central PPV core in which two aliphatic chains are connected through the pyridinium ends (**1**–**4**). In a two-step procedure, different alkyl chains of desired lengths were first covalently attached to 4-picoline by means of quarternization. Then each pyridinium salt was subjected to a base-induced aldol-type condensation with terephthalaldehyde to furnish the final product (see the Experimental Sec-

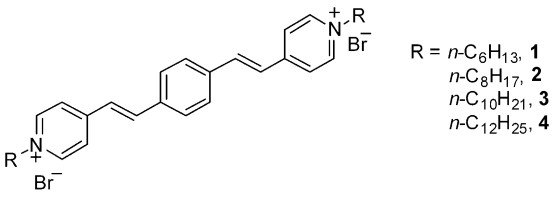

[a] Prof. Dr. S. Bhattacharya, Dr. S. K. Samanta
Department of Organic Chemistry
Indian Institute of Science
Bangalore 560012, Karnataka (India)
Fax: (+91) 80-23600529
E-mail: sb@orgchem.iisc.ernet.in

[b] Prof. Dr. S. Bhattacharya
Chemical Biology Unit
Jawaharlal Nehru Centre for Advanced Scientific Research
Bangalore 560064, Jakkur (India)

Supporting information for this article is available on the WWW under http://dx.doi.org/10.1002/chem.201201940.

tion). Each compound was characterized unambiguously by using FTIR spectroscopy, ^{1}H and ^{13}C NMR spectroscopy, mass spectrometry, and elemental analysis. The presence of an all-*trans* configuration of the two vinyl moieties in **1**–**4** was confirmed from the ^{1}H NMR spectra ($J \approx 16$ Hz; Figure S1 in the Supporting Information).

Gelation studies and gel-melting temperatures: Each compound was dispersed in water and only compound **2** formed an excellent hydrogel. Compound **1** precipitated and the one with longer chains (**3**) showed a propensity for aggregation, whereas **4** was found to be sparingly soluble in water. This indicates that a crucial hydrophobic/hydrophilic balance[8] in **2** with two *n*-octyl chains is responsible for its gelation in water with a minimum gelator concentration (MGC) of 1.76 mM (0.12 wt%). Thus, one molecule of **2** could gelate as many as approximately 30000 water molecules, which deserves to belong to the category of 'supergelators'.[9] The gel melting temperature (T_{gel}), obtained by the dropping ball method,[10] increased with increasing concentrations of **2** (Figure 1a). This indicates that with increasing gelator concentration, the density of the gel assembly increases to ensure participation of a larger number of gelator molecules per unit volume in the thermally induced transitions.[11] The increase in T_{gel} reached a plateau at a concentration of approximately 7.5 mM. Beyond this, the addition of further compounds into the mixture could not be solubilized either by heating and/or sonicating.

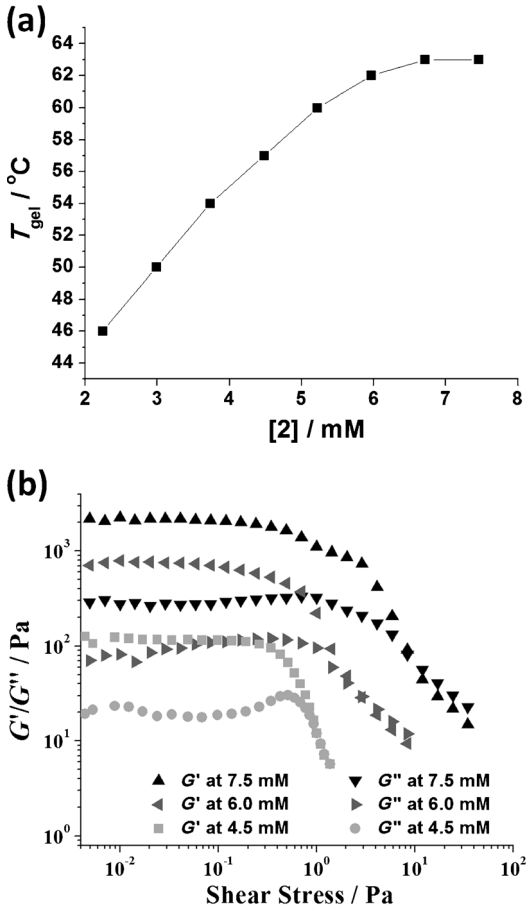

Figure 1. a) Plot of T_{gel} versus concentration of **2** in water. b) Dynamic stress amplitude sweep of the hydrogels with increasing concentration of **2**.

Mechanical behavior of the gels: Rheological experiments show an elastic response of the gels under applied external mechanical stress. Rotational flow curve experiments show that with increasing shear rate, the viscosity of the gel decreases linearly (slope approaching −1), thus indicating that this gel is a shear thinning material (Figure S2a in the Supporting Information).[12] Under oscillatory stress amplitude, the gels show an eightfold higher elastic modulus (G') than the viscous modulus (G''), thus indicating a dominant solidlike behavior (Figure 1b).[12b] The yield stress (σ_y), an applied stress above which the gel starts to flow, increased with increasing concentration. The oscillatory frequency response of the gel reveals that G' is independent of frequency over the entire angular frequency range (1–100 rad s^{-1}) at 0.01% strain amplitude. The viscoelastic solidlike nature of the gels increased with increasing concentration of **2** and it became sufficiently strong ($G' \approx 2200$ Pa at 7.5 mM), which did not relax over the long timescale of the experiment (Figure S2b in the Supporting Information).[12c]

^{1}H NMR spectroscopic studies of the gel: ^{1}H NMR spectroscopic study of a gel of **2** in D_2O was performed at different temperatures to understand the nature of interactions that are responsible for the thermoreversible gelation. In the gel, the ^{1}H NMR spectroscopic signals broadened and almost quenched owing to the restriction of the molecular tumbling to produce zero-average dipolar coupling.[13] Upon increasing the temperature as the gel melted progressively, an isotropic distribution of the molecules was achieved in solution and their NMR spectroscopic signals started to appear gradually (Figure S3 in the Supporting Information). Well-resolved peaks were observed above the T_{gel} (≈ 46 °C for 2.2 mM of **2**). A concomitant increase in the δ values with increasing temperature indicates deshielding of the ^{1}H signals upon breakdown of the self-assembly. This indicates that the self-assembly might be promoted by the π–π-stacking interactions, and that participation of both aromatic and aliphatic protons are responsible for the gel formation.[13b–d]

Morphology under the microscope: Morphological studies showed their topography in the gel matrix. Under a fluorescence microscope, a thin film of **2** showed yellow emission and the presence of three-dimensional fiber bundles approximately 1–2 μm in diameter was observed when excited at 340–400 nm (Figure 2a). SEM images of the xerogel ensured the presence of a fibrillar network with a fiber diameter of approximately 1–2 μm. Interestingly, the SEM images also showed the presence of a coil-type morphology distributed throughout the sample along with the fibers (Figure 2b,c). A magnified image clearly shows the formation of the coils by further assemblage of the individual fibers. Also, the individ-

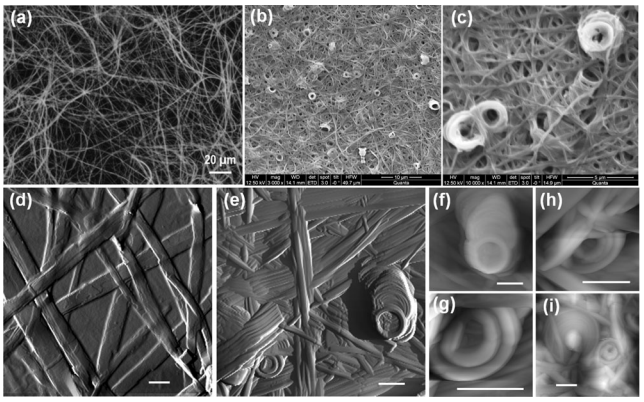

Figure 2. a) Fluorescence microscopy image of a thin film of **2** (1 mM; scale bar: 20 μm); b) SEM image of a xerogel of **2** (3 mM; scale bar: 10 μm) and c) its magnified image (scale bar: 5 μm). d,e) AFM amplitude and f–j) topography images of the thin film of **2** obtained from d) the sol (0.75 mM) and e–i) the gel (3 mM); scale bars: 1 μm in each case).

ual coils combined together appear to form a tube with shorter aspect ratio. AFM images confirmed the appearance of the coil-type morphology above the MGC concentration of **2** (Figure 2d–i). A thin film of **2** obtained from a 'sol' (0.75 mM) in water showed only the presence of fibers of high aspect ratio. This excludes the possibility of coil formation during solvent evaporation from the gels. The gel (3 mM) showed the presence of both the fiber and coil-type morphologies throughout the sample. The coils were of almost uniform diameter (≈1 μm) and were polymorphic in nature. Concentric circular coils were observed to have various numbers of layers (2, 3, or multiple). Clearly, multiple coils were assembled together to lead to the formation of a tube.[14]

Packing pattern of the gelator molecules: X-ray diffraction studies of the xerogel showed repetitive Bragg reflection peaks, thus indicating a lamellar-type arrangement in the supramolecular self-assembly (Figure 3a).[15] The intense first Bragg peak at 2.55 nm indicates a repetitive unit of **2** that is nearly the double of the calculated aliphatic chain length of the energy-minimized structure (Figure S4 in the Supporting Information). The crystalline lamellar fibers showed birefringent textures under a polarized optical microscope, thus indicating an anisotropic packing of the PPV molecules[16] either in the thin film or in the hydrogel (Figure S5 in the Supporting Information). A model might be proposed by summing up all of these observations in a way that consists of π stacking among the aromatic parts and van der Waals interactions through the *n*-octyl chains in a repetitive manner in its self-assembly (Figure 3b). The repulsion between charged pyridinium units might be mitigated by the extensive hydration and partially slipped cation–π interactions might further facilitate the self-organization by minimizing the charge repulsion.

Photophysical properties of gels and solutions: This class of molecules is chromophoric, which allows for the evaluation

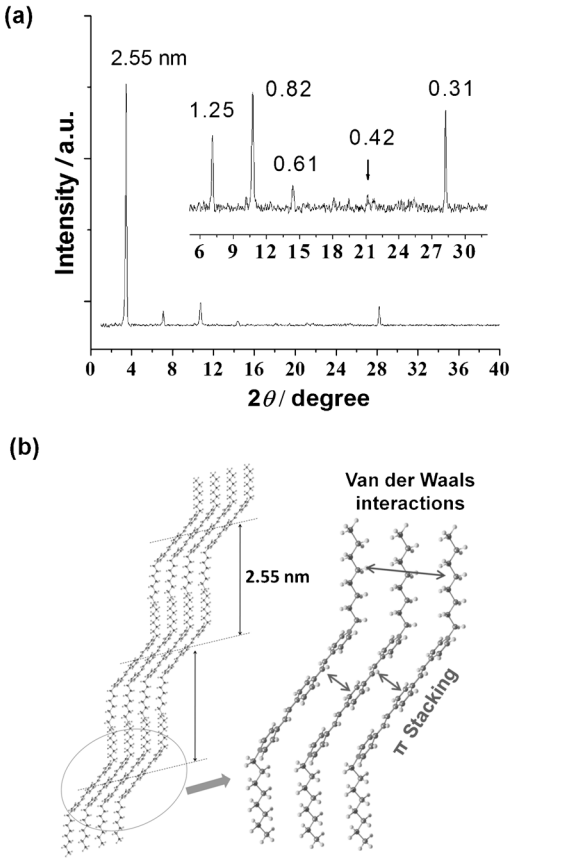

Figure 3. a) XRD patterns of **2** (3 mM) with an inset showing the magnified plot and b) probable self-organization and the molecular interactions between molecules of **2**.

of their optical and photophysical properties.[17] The UV/Vis absorption spectra (Figure 4a) of a dilute solution of **2** (20 μM) in water showed a maximum at 395 nm ($S_0 \rightarrow S_1$, $\varepsilon = 58\,500\ cm^{-1}M^{-1}$) along with a small band at 247 nm ($S_0 \rightarrow S_2$). The same solution showed an emission maximum at 470 nm when excited at 380 nm, which represents their 'monomeric' emission (Figure 4b). Interestingly, a drastic change in color was observed from a sol to a gel of **2** (4 mM) either under UV (365 nm) or normal daylight (Figure 5a). Thus, the photophysical properties in the gel state (aggregated species) are vastly different from those in the solution (monomeric species). This could be a consequence of aggregation in water. Indeed, the aggregation of **2** in solution was accomplished upon the addition of a salt with the common ion (Br^-). Thus, when a solution of NaBr was added to the aqueous solution of **2** (20 μM), the color of the solution changed immediately and matched with that of the gel under normal or UV light, thereby ensuring that an aggregated state was achieved (Figure 5b). The added NaBr might have caused a disruption in the hydration of **2** around the pyridinium centers. The increase in the ionic strength of the solution affects the delicate hydrophilic/hydrophobic balance of **2** in solution, thus leading to the aggregation.

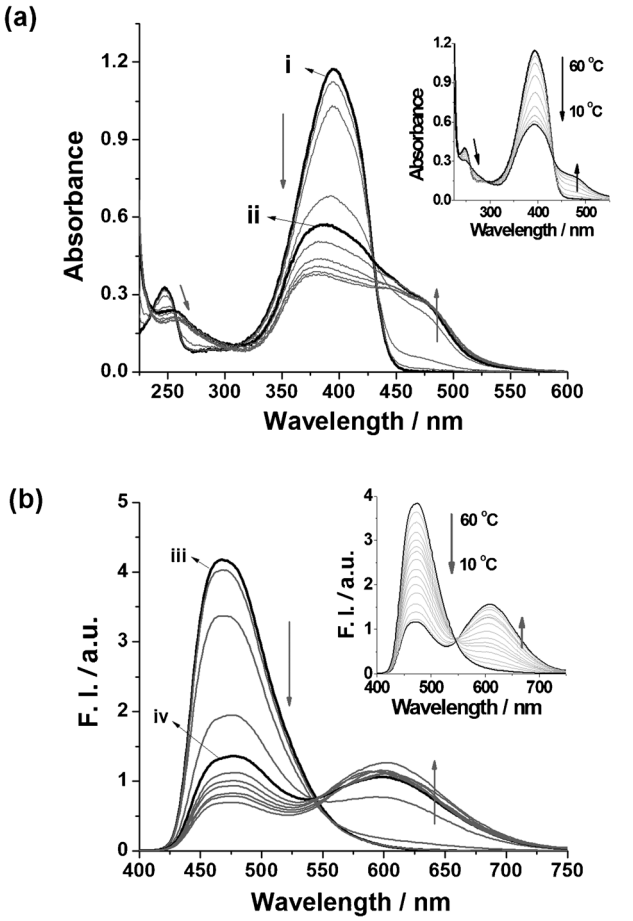

Figure 4. a) UV/Vis and b) fluorescence spectra showing titration of **2** (20 μM) in water with NaBr (5 mM NaBr added each time), insets of (a) and (b) show thermoreversible aggregation of **2** in the presence of 20 and 30 mM NaBr, respectively. Absorption and emission spectra show i, iii) monomeric and ii, iv) aggregated species in the presence of 20 mM NaBr, respectively.

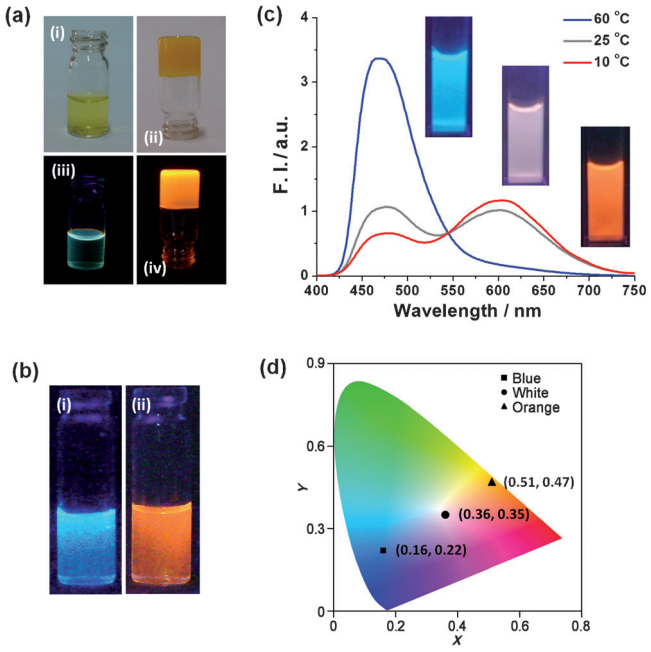

Figure 5. a) Thermoreversible sol/gel phenomenon of **2** (4 mM) in water shown under i, ii) daylight and iii, iv) 365 nm UV light. The sky-blue emission of the sol is a result of the monomeric species and the orange emission of the gel is a result of the aggregated gelator molecules. b) Aggregation of **2** (20 μM) in the solution phase upon addition of NaBr (50 mM) showing changes in the emission from sky-blue to orange at room temperature. c) Aggregation-induced emission switches of **2** (20 μM) containing 30 mM of NaBr at different temperatures in the solution phase. Insets show the corresponding emission colors under a 365 nm UV lamp. d) CIE 1931 chromaticity diagram for the sky-blue, white, and orange emission.

Effect of salt on the aggregation in solution: To probe this salt-induced aggregation phenomenon, a solution of **2** (20 μM) in water was titrated with a stock solution of NaBr (1 M; Figure 4a). Under UV/Vis spectroscopy, the intensity of the 395 nm band decreased progressively along with the appearance of a new band at 480 nm owing to the onset of an aggregated state. An optimum aggregation was achieved when the concentration of NaBr in the final solution reached 20 mM, whereas the 480 nm band did not show any significant changes. Beyond this concentration, further addition of NaBr only led to decreases in the 395 nm band, and it finally reached a point of saturation at approximately 40 mM of NaBr.

The solution of **2** (20 μM) that contained 20 mM NaBr was then subjected to temperature variations. At higher temperature (60 °C), the spectra resembled that of a monomeric absorption (Figure 4a, inset). When the temperature was lowered, the intensity of the 395 nm band decreased and the hump at 480 nm increased progressively until it saturated at approximately 10 °C. The presence of a clear isosbestic point at 432 nm indicates the existence of a thermoreversible equilibrium between the monomeric and the aggregated states.

Aggregation-induced emission switches: When the fluorimetric titration was carried out, the intensity of the monomeric emission at 470 nm decreased along with the appearance of an aggregated emission band at 600 nm (Figure 4b).[18] The 600 nm band reached saturation upon addition of 20 mM of NaBr and a further decrease in the 470 nm band was observed upon gradual addition of NaBr. When the temperature of the solution of **2** (20 μM) that contained 30 mM of NaBr was decreased, the aggregated emission band at 600 nm emerged gradually with a concomitant decrease in the monomeric emission (470 nm), thereby ensuring the thermoreversibility phenomenon (Figure 4b, inset). Therefore, the addition of salt and variation in temperature mimic the sol–gel-induced self-assembly process. When these titrated solutions were viewed under a 365 nm UV lamp, a transition from sky-blue emission (due to the monomeric species) to orange emission (due to the aggregated species) was observed by means of white-light emission with increasing salt concentrations (Figure S7 in the Supporting Information). Also, the solution of **2** that contained 30 mM NaBr showed a sky-blue emission at higher temperature (>50 °C), an orange emission at low temperature (<15 °C),

and a white-light emission at room temperature (25–30 °C; Figure S8 in the Supporting Information). Thus, either by varying the concentration of NaBr or the temperature of the solution, different emission could be achieved depending on the extent of aggregation of the monomers (Figure 6).

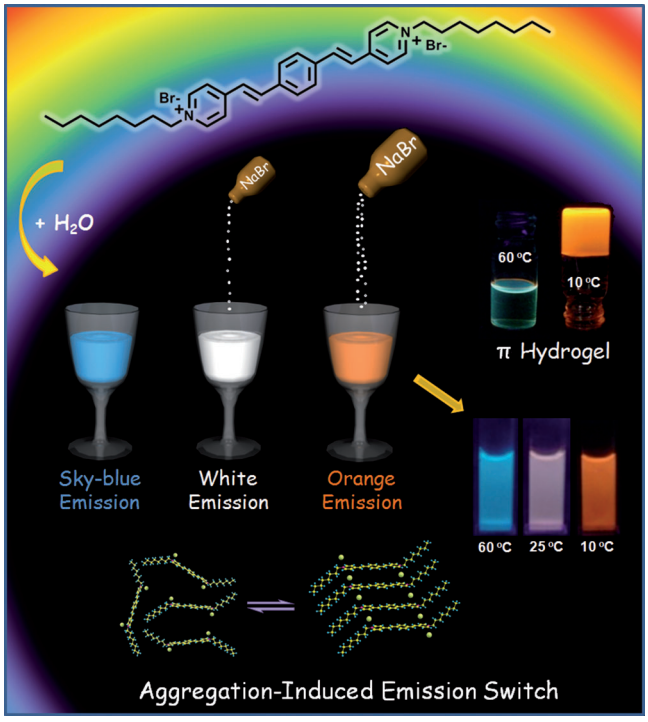

Figure 6. A graphical representation depicting the salt-induced switch of the emission colors, which resembles the disorder-to-order-induced sol–gel transition. The sky-blue emission of the gelator alone in water transformed into white light followed by orange emission upon progressive addition of NaBr at room temperature. The orange emissive solution exhibits further emission switches upon temperature variation under a 365 nm UV lamp. The monomeric sky-blue emission and the aggregated orange emission matched with that of the sol and gel, respectively, as a consequence of the reversible order–disorder transitions.

White-light emission: We also recorded the excitation and emission spectra for the same solution (20 μM of **2** that contained 30 mM of NaBr) at 10, 25, and 65 °C after a visual preview of their emission color under a 365 nm UV lamp. The emission spectra were consistent with the previous observations and resembled that of a monomeric emission (470 nm) at 60 °C, an aggregated emission (600 nm) at 10 °C, and a wide-range emission (≈425–700 nm) at 25 °C (Figure 5c). At 60 °C, only monomeric emission appeared and the band corresponding to the aggregated emission was absent. At 10 °C, the intensity of the aggregated emission band was predominant over the monomeric band. However, at room temperature, the intensity of both the bands was comparable and it covered almost the whole visible spectral region, thus leading to a white-light emission through a mixture of both monomers and aggregates in the solution. The CIE chromaticity diagram exhibited the coordinates for the white-light emission (0.36, 0.35; Figure 5d), which are quite close to those of pure white-light emission (0.33, 0.33). The corresponding excitation spectra also supports the aggregation-induced emission switches, and it resembled the variable-temperature absorption spectra (Figure S9 in the Supporting Information). Thus, the temperature variation operated as an emission 'switch', and the aggregation-induced white-light emission from a single component in a single solvent makes the system potentially useful for optoelectronic applications. Other instances also bring about such effects but notably require a mixture of two or more components and/or solvents.[19] Therefore, our findings demonstrate that white-light emission can be obtained from a single chromophore, which is always more desirable than that of a mixture of chromophoric systems.

Fluorescence decay profiles of **2** were recorded in aqueous solution, as a hydrogel, and in the presence of NaBr at different temperatures for the monomeric species, the aggregated species, and the mixture (Figure S10 in the Supporting Information). In solution, compound **2** (20 μM) showed a monoexponential fluorescence decay with a time constant of 0.1 ns ($\chi^2=1.06$) when the emission was recorded at 470 nm (Table S1 in the Supporting Information). The hydrogel of **2** (3 mM) showed a multiexponential decay ($\lambda_{em}=600$ nm) with the time constants of 4.7 (17 %), 16.5 (70 %), and 0.6 ns (13 %), with an average lifetime of 15.5 ns ($\chi^2=1.18$).

The fluorescence decay curves for a solution of **2** (20 μM) that contained 30 mM of NaBr at 60 (sky-blue emission), 25 (white emission), and 10 °C (orange emission) were recorded at two different wavelengths (470 and 600 nm). When recorded at 470 nm (at a monomeric emission band), a monoexponential decay was observed in each case (Table S1 in the Supporting Information). However, multiexponential decay curves were obtained when the emission was recorded at 600 nm (aggregated emission band) with average lifetimes of 5.9 ns ($\chi^2=1.05$) at 60 °C, 7.0 ns ($\chi^2=1.09$) at 25 °C, and 7.3 ns ($\chi^2=1.03$) at 10 °C. The increase in lifetime values as temperature decreased might be a result of the appearance of relatively long-lived species that are formed owing to the salt-induced aggregation of the gelator molecules.[20]

Effect of other salts and Hofmeister series: To investigate the role of addition of various inorganic salts on the aggregation behavior of **2** in water, titration was carried out by systematically varying the anions and then the cations as well (Figure S11 in the Supporting Information). Among the anions, SCN^- showed the highest activity in terms of quenching of the monomeric emission at 470 nm relative to the other anions examined (NO_3^-, SO_4^{2-}, I^-, Br^-, Cl^-, and F^-). The addition of approximately 2 mM NaSCN into an aqueous solution of **2** (20 μM) showed an effective quenching of the monomeric emission, which led to the onset of an aggregated emission at 600 nm. Among the halide series (F^-, Cl^-, Br^-, and I^-), iodide appeared to be the strongest quencher and an optimum quenching occurred with approximately 6 mM of NaI. Interestingly, although an efficient quenching was observed with NaI, it did not produce the aggregated emission band. This might be a result of the large

ionic radius of I^-, which did not allow the molecules of **2** to come in direct proximity to impart efficient π-stacking interactions between the PPV aromatic units (see below). $NaNO_3$ (≈10 mM) showed a greater quenching efficiency than NaBr (≈40 mM). However, Na_2SO_4, NaCl, and NaF showed negligible quenching. Under a 365 nm UV lamp, these titrated solutions showed emission consistent with the above observations (Figure S12d in the Supporting Information). The fluorescence emission of the aggregated band at 600 nm was more intense in the case of $NaNO_3$, which produced a stronger yellow emission in the UV chamber than NaSCN. This might be a result of a planar geometry of the NO_3^- ions. The emission color was quenched in the case of NaI, since iodide is known to be a strong quencher.[21] However, the emission color upon individual addition of Na_2SO_4, NaCl, and NaF resembled that of the monomeric emission.

We then determined the Stern–Volmer quenching constant (K_{SV}) on the basis of the titration of **2** with different anions. Here **2** acted as a fluorophore and the added salt as a quencher. K_{SV} indicates the sensitivity of a fluorophore to a quencher and has been calculated by using Equation (1):[22]

$$\frac{F_0}{F} = 1 + K_{sv}[Q] \qquad (1)$$

in which F_0 and F are the emission intensities of the fluorophore in the absence and presence of a quencher and [Q] is the concentration of the quencher [mM]. A plot of F_0/F as a function of [Q] yields a straight line, the slope of which affords the K_{SV} value (Figure S12 in the Supporting Information). The K_{SV} values follow the order $SCN^- > I^- > NO_3^- > Br^- > SO_4^{2-} > Cl^- > F^-$ (Table S2 in the Supporting Information). These indicate that the relative ability of each anion to quench the fluorescence emission of **2** is in agreement with the known Hofmeister series, a trend of ions that governs the folding/unfolding of proteins and other macromolecules in aqueous media.[23] Therefore, this observation suggests that the same trend could also hold true for the small molecules.

The effect of cations on the aggregation of **2** in water was also checked with a fixed anion (Cl^-), which, however, had a less pronounced effect on the aggregation process. With increasing cationic charge, aggregation increased and followed the order $Ca^{2+} > Mg^{2+} > K^+ > Na^+ > Li^+$, which is also in agreement with the Hofmeister series.

Thus, addition of either anions or cations leads to the changes in the assembly of **2** in water, and it is more pronounced for the anions than the cations. For cations, the extent of self-assembly depends on the number of cationic charges that modify the extent of hydration of **2**. The extent of aggregation for the anions thus clearly depends primarily on two factors: 1) the anion exchange with the preexisting Br^- counterions followed by 2) the extent of hydration of the resulting mixture that contains the replaced anions. Therefore, the observed Hofmeister series is a result of the direct interactions of the ions with the gelator molecules followed by hydration of the resulting system, which is primarily responsible for the aggregation and not indirect influences that occur through changes in the water structure.[23b] To address this, anion displacement studies were also undertaken.

Anion-exchange studies: The anion displacement was studied by adding one anion followed by titration with the other (Figure 7). This also explains the mechanism of the aggregation process at the molecular level. Although addition of I^- (10 mM) into an aqueous solution of **2** (20 μM) shows fluorescence quenching, it resembles only monomeric emission (470 nm). However, addition of NaSCN (10 mM) into this solution led to the aggregated emission at 600 nm. This indicates that SCN^- can replace I^- as the counterion, and the resulting species gives rise to the aggregated state. When the titration was performed in the reverse order, that is, when the solution of **2** that contained NaSCN (10 mM) was titrated with NaI, the aggregates could not be broken into the monomeric species; only a fluorescence quenching was observed. This also excludes the possibility of the simple heavy-atom effect of I^-, since it could only quench the emission and not break the aggregation. Addition of NO_3^- or Br^- to the solution of **2** that contained NaI did not show noticeable extent of aggregation except for a large excess amount of Br^-. However, the addition of I^- to the solution of **2** in its aggregated state, which was achieved either by the

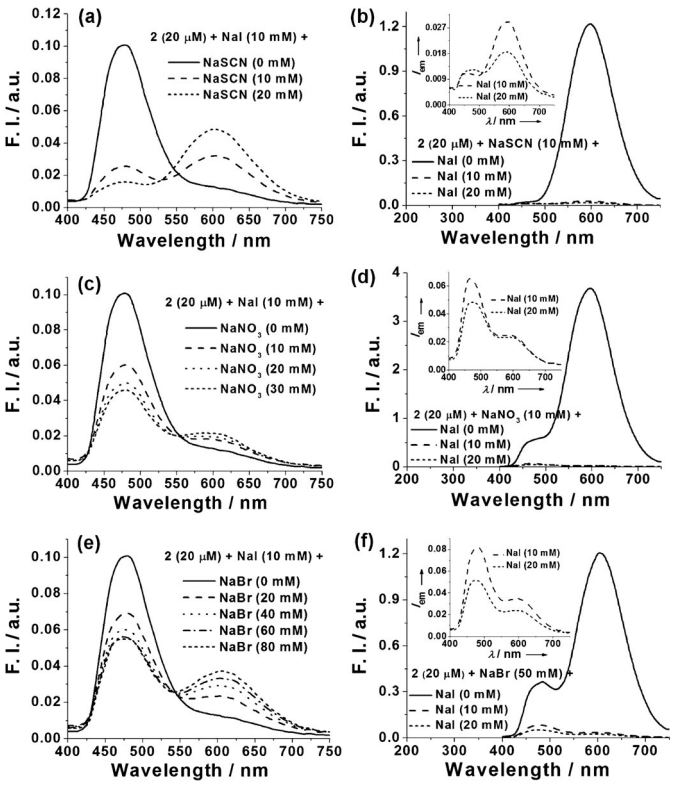

Figure 7. Effects on fluorescence emission upon exchange of anion: a) NaI with NaSCN, b) NaSCN with NaI, c) NaI with $NaNO_3$, d) $NaNO_3$ with NaI, e) NaI with NaBr, and f) NaBr with NaI. Insets show the magnification of the quenched spectra.

addition of Br^- or NO_3^-, led to the breakdown of the assembly in both instances. These observations indicate that the anion exchange also follows the Hofmeister series.

The above phenomena might be explained by the model depicted in the Figure 8. It is believed that in the presence of anions such as SCN^-, NO_3^-, or Br^-, self-assembly is achieved through π stacking, and the anions are placed between the PPV units. However, as the size of the anion becomes larger, as in the case of I^-, it does not facilitate the π stacking between the PPV units, and hence aggregation-induced emission at 600 nm was not observed.

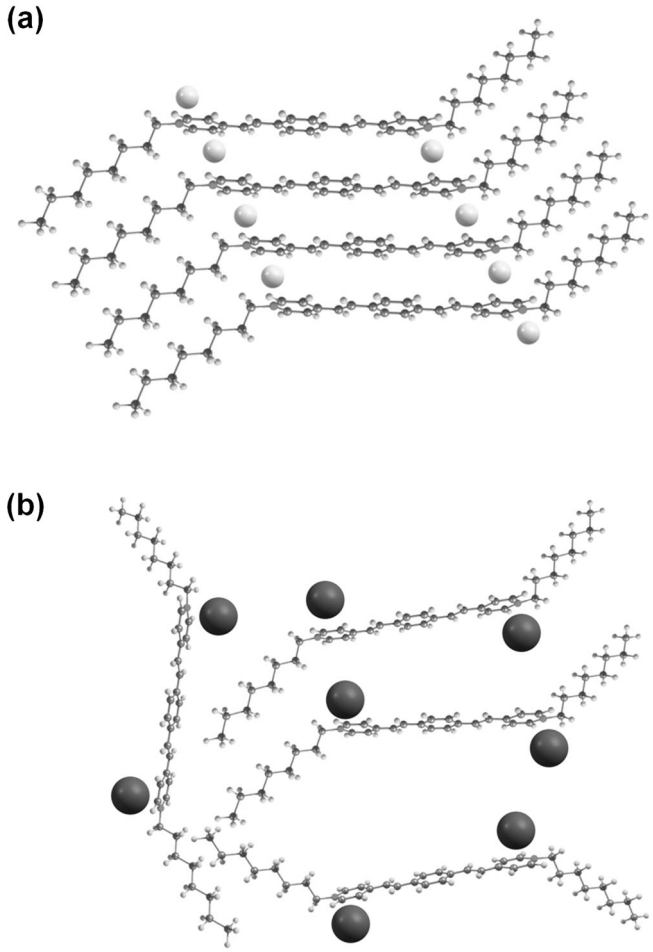

Figure 8. Probable self-organization motifs of **2** dictated by a) Br^- (gray spheres) and b) I^- (black spheres) ions.

For anions such as F^-, Cl^-, or SO_4^{2-}, the anion replacements do take place. But due to the greater extent of hydration, the hydrophilic/hydrophobic balance could not be maintained for their optimal self-organization in water. However, for SCN^-, NO_3^-, or Br^- after their anion replacement, the hydrophobic effects dominate on account of a lesser degree of hydration, thus leading them to the aggregated state. Additional hydration of the added salts in aqueous media also helps the PPV to aggregate further, and therefore when **2** was titrated with NaBr, it led to a higher state of aggregation.

Conclusion

In summary, the collective analyses demonstrate the self-organization propensity of **2** in water, thereby leading to hydrogel formation through the optimization of π-stacking, van der Waals, and electrostatic interactions. Variation in the added salt type, concentration, or temperature profoundly influenced the aggregation of **2** in aqueous solution. Formation of a novel chromophore assembly in this way leads to an aggregation-induced switch of emission colors. Thus, a sky-blue emission at $>50\,°C$, an orange emission at $<15\,°C$, and a white-light emission at room temperature (25–30 °C) were observed. To the best of our knowledge, this is the first observation of the control of aggregation and emission switches of LMMGs by using different salts that follow the well-known Hofmeister series. Mechanistic insights for the aggregation process (through anion exchange and alteration in hydration in this case) would be helpful to explore these kinds of π gelators. The aggregation-induced emission that shows room-temperature white-light emission from a single chromophore in a single solvent (water) makes the system useful for optoelectronic applications. Furthermore, pharmacological usefulness of this type of charged (cationic/anionic) conjugated molecule[6b,7] adds to the potential of these new bis-cationic phenylenevinylenes for cellular imaging of events involved in killing bacteria and viruses. Investigative work is underway in this direction in our laboratory.

Experimental Section

Materials and methods: All reagents and solvents were obtained from the best-known commercial sources and were used without further purification. FTIR studies were performed using a Perkin–Elmer FTIR Spectrum BX system and were reported in wavenumbers [cm^{-1}]. ^1H and ^{13}C NMR spectra were recorded using a Bruker 400 Avance NMR spectrometer. Chemical shifts were reported downfield from the internal standard, tetramethylsilane. Mass spectrometry of individual compounds was performed using a MicroMass ESI-TOF MS instrument. Elemental analysis was recorded using a Thermo Finnigan EA FLASH 1112 SERIES instrument.

Synthesis and characterization: Compound **2** was synthesized upon appropriate modification of the reported literature procedure.[17a,b] A mixture of *n*-octyl bromide and 4-picoline (1:2 mol) was heated to reflux in ethanol for 12 h to obtain the corresponding 4-picolinium salt. Then the reaction mixture was cooled and an excess amount of 4-picoline was removed under vacuum followed by repeated washing with hexane to give rise to a white solid. The 4-picolinium salt thus obtained and terephthalaldehyde were dissolved in a 2:1 molar ratio in ethanol, and an aqueous solution (2 mL) of K_2CO_3 (2 equiv) was added dropwise into the ethanol solution under ice-cold conditions. The mixture was stirred under ice-cold conditions for 2 h, and then the reaction was quenched by acidification with 3 N HCl. Ethanol was removed under vacuum, and the precipitate was filtered and washed with ice-cold water. The crude product was dissolved in methanol and precipitated in ethyl acetate, followed by filtration to obtain a yellow solid. This cycle was repeated several times

until the pure product was obtained as indicated from TLC. A similar method was used to prepare compounds **1**, **3**, and **4**.

4,4′-[(1*E*,1′*E*)-1,4-Phenylenebis(ethene-2,1-diyl)]bis(1-hexyl pyridinium) bromide (1): Yield 26%; ^{1}H NMR (500 MHz, CD_3OD): $\delta = 0.91$–0.93 (t, 6H; CH_3), 1.27–1.38 (m, 12H; CH_2), 2.01 (m, 4H; N^+-CH_2-CH_2), 4.54 (t, 4H; N^+–CH_2), 7.53–7.56 (d, $J = 16.5$ Hz, 2H; vinylic), 7.86 (s, 4H; aromatic), 7.96–7.99 (d, $J = 16.0$ Hz, 2H; vinylic), 8.21- 8.22 (d, $J = 6.0$ Hz, 4H; aromatic), 8.82–8.83 ppm (d, $J = 6.0$ Hz, 4H; aromatic); ^{13}C NMR (125 MHz, CD_3OD): $\delta = 14.23$, 23.46, 26.89, 32.29, 32.32, 62.04, 125.30, 125.59, 128.69, 130.11, 130.83, 138.64, 141.85, 145.35, 155.20 ppm; FTIR (neat): $\tilde{\nu}_{max} = 2926$, 2851, 1615, 1522, 1479, 1359, 1209, 1172, 996, 874, 726 cm^{-1}; TOF-MS: *m*/*z* calcd for $C_{32}H_{42}N_2^{2+}$: 227.1674; found: 227.1676; elemental analysis calcd (%) for $C_{32}H_{42}N_2Br_2$: C 62.55, H 6.89, N 4.56; found: C 62.63, H 6.88, N, 4.84.

4,4′-[(1*E*,1′*E*)-1,4-Phenylenebis(ethene-2,1-diyl)]bis(1-octyl pyridinium] bromide (2): Yield 29%; ^{1}H NMR (500 MHz, CD_3OD): $\delta = 0.88$–0.90 (t, 6H; CH_3), 1.30–1.39 (m, 20H; CH_2), 2.01 (m, 4H; N^+-CH_2-CH_2), 4.54 (t, 4H; N^+–CH_2), 7.53–7.56 (d, $J = 16.0$ Hz, 2H; vinylic), 7.86 (s, 4H; aromatic), 7.96–8.00 (d, $J = 16.5$ Hz, 2H; vinylic), 8.21- 8.22 (d, $J = 6.5$ Hz, 4H; aromatic), 8.82–8.83 ppm (d, $J = 6.5$ Hz, 4H; aromatic); ^{13}C NMR (125 MHz, CD_3OD): $\delta = 14.38$, 23.65, 27.22, 30.09, 30.18, 32.38, 32.86, 62.03, 125.29, 125.57, 130.11, 138.63, 141.83, 145.35, 155.17 ppm; FTIR (neat): $\tilde{\nu}_{max} = 2920$, 2852, 1615, 1519, 1468, 1353, 1328, 1210, 1173, 979, 847, 723 cm^{-1}; TOF-MS: *m*/*z* calcd for $C_{36}H_{50}N_2^{2+}$: 255.1987; found: 255.1985; elemental analysis calcd (%) for $C_{36}H_{50}N_2Br_2{\cdot}2H_2O$: C 61.19, H 7.70, N 3.96; found: C 61.35, H 8.02, N 4.18.

4,4′-[(1*E*,1′*E*)-1,4-Phenylenebis(ethene-2,1-diyl)]bis(1-decyl pyridinium) bromide (3): Yield 30%; ^{1}H NMR (400 MHz, CD_3OD): $\delta = 0.86$–0.89 (t, 6H; CH_3), 1.28–1.39 (m, 28H; CH_2), 1.99–2.02 (m, 4H; N^+-CH_2-CH_2), 4.52–4.56 (t, 4H; N^+–CH_2), 7.52–7.56 (d, $J = 16.4$ Hz, 2H; vinylic), 7.86 (s, 4H; aromatic), 7.96–8.00 (d, $J = 16.0$ Hz, 2H; vinylic), 8.21–8.23 (d, $J = 6.8$ Hz, 4H; aromatic), 8.82–8.84 ppm (d, $J = 7.2$ Hz, 4H; aromatic); ^{13}C NMR (100 MHz, CD_3OD): $\delta = 14.40$, 23.70, 27.21, 30.11, 30.37, 30.49, 30.56, 32.36, 33.02, 62.05, 125.30, 125.59, 130.11, 130.83, 138.64, 141.86, 145.35, 155.19 ppm; FTIR (neat): $\tilde{\nu}_{max} = 2919$, 2850, 1615, 1469, 1353, 1329, 1211, 1176, 978, 847, 722 cm^{-1}; TOF-MS: *m*/*z* calcd for $C_{40}H_{58}N_2^{2+}$: 283.2300; found: 283.2301; elemental analysis calcd (%) for $C_{40}H_{58}N_2Br_2$: C 66.11, H 8.04, N 3.85; found: C 66.10, H 8.21, N 3.77.

4,4′-[(1*E*,1′*E*)-1,4-Phenylenebis(ethene-2,1-diyl)]bis(1-dodecyl pyridinium) bromide (4): Yield 35%; ^{1}H NMR (400 MHz, CD_3OD): $\delta = 0.86$–0.89 (t, 6H; CH_3), 1.22–1.39 (m, 36H; CH_2), 1.99–2.02 (m, 4H; N^+-CH_2-CH_2), 4.52–4.55 (t, 4H; N^+–CH_2), 7.52–7.56 (d, $J = 16.4$ Hz, 2H; vinylic), 7.86 (s, 4H; aromatic), 7.95–7.99 (d, $J = 16.0$ Hz, 2H; vinylic), 8.20–8.22 (d, $J = 6.8$ Hz, 4H; aromatic), 8.81–8.83 ppm (d, $J = 6.8$ Hz, 4H; aromatic); ^{13}C NMR (100 MHz, CD_3OD): $\delta = 14.41$, 23.72, 27.21, 30.11, 30.45, 30.48, 30.60, 30.72, 32.36, 33.06, 62.06, 125.03, 125.31, 125.59, 128.69, 130.12, 130.83, 138.65, 141.86, 145.36, 155.21 ppm; FTIR (neat): $\tilde{\nu}_{max} = 2918$, 2849, 1617, 1520, 1467, 1353, 1329, 1211, 1175, 979, 846, 722 cm^{-1}; TOF-MS: *m*/*z* calcd for $C_{44}H_{66}N_2^{2+}$: 311.5041; found: 311.3030; elemental analysis calcd (%) for $C_{44}H_{66}N_2Br_2$: C 67.51, H 8.50, N 3.58; found: C 67.53, H 8.77, N 3.43.

Acknowledgements

We thank the DST for financial support, and INI and the Department of Physics for various instrumental facilities. S.K.S is grateful to CSIR for a Senior Research Fellowship. S.B. thanks the DST for a J.C. Bose Fellowship.

[1] a) P. Terech, R. G. Weiss, *Chem. Rev.* **1997**, *97*, 3133–3159; b) T. Ishi-I, S. Shinkai, *Top. Curr. Chem.* **2005**, *258*, 119–160; c) S. Bhattacharya, S. K. Samanta, *Langmuir* **2009**, *25*, 8378–8381.

[2] a) M. Llusar, C. Sanchez, *Chem. Mater.* **2008**, *20*, 782–820; b) S. Yagai, S. Mahesh, Y. Kikkawa, K. Unoike, T. Karatsu, A. Kitamura, A. Ajayaghosh, *Angew. Chem.* **2008**, *120*, 4769–4772; *Angew. Chem. Int. Ed.* **2008**, *47*, 4691–4694.

[3] a) T. Goodson, III, W. Li, A. Gharavi, L. Yu, *Adv. Mater.* **1997**, *9*, 639–643; b) F. Würthner, *Chem. Commun.* **2004**, *14*, 1564–1579; c) S. S. Babu, S. Prasanthkumar, A. Ajayaghosh, *Angew. Chem.* **2012**, *124*, 1800–1810; *Angew. Chem. Int. Ed.* **2012**, *51*, 1766–1776.

[4] a) M. Ikeda, M. Takeuchi, S. Shinkai, *Chem. Commun.* **2003**, 1354–1355; b) J. F. Hulvat, M. Sofos, K. Tajima, S. I. Stupp, *J. Am. Chem. Soc.* **2005**, *127*, 366–372; c) S.-J. Yoon, J. H. Kim, J. W. Chung, S. Y. Park, *J. Mater. Chem.* **2011**, *21*, 18971–18973; d) S. Srinivasan, P. A. Babu, S. Mahesh, A. Ajayaghosh, *J. Am. Chem. Soc.* **2009**, *131*, 15122–15123; e) K. K. Kartha, S. S. Babu, S. Srinivasan, A. Ajayaghosh, *J. Am. Chem. Soc.* **2012**, *134*, 4834–4841.

[5] a) A. El-ghayoury, A. P. H. J. Schenning, P. A. van Hal, J. K. J. van Duren, R. A. J. Janssen, E. W. Meijer, *Angew. Chem.* **2001**, *113*, 3772–3775; *Angew. Chem. Int. Ed.* **2001**, *40*, 3660–3663; b) A. Ajayaghosh, S. J. George, *J. Am. Chem. Soc.* **2001**, *123*, 5148–5149; c) A. P. H. J. Schenning, J. V. Herrikhuyzen, P. Jonkheijm, Z. Chen, F. Wurthner, E. W. Meijer, *J. Am. Chem. Soc.* **2002**, *124*, 10252–10253; d) F. J. M. Hoeben, I. O. Shklyarevskiy, M. J. Pouderoijen, H. Engelkamp, A. P. H. J. Schenning, P. C. M. Christianen, J. C. Maan, E. W. Meijer, *Angew. Chem.* **2006**, *118*, 1254–1258; *Angew. Chem. Int. Ed.* **2006**, *45*, 1232–1236; e) M. Mba, A. Moretto, L. Armelao, M. Crisma, C. Toniolo, M. Maggini, *Chem. Eur. J.* **2011**, *17*, 2044–2047; f) C. Löwe, C. Weder, *Adv. Mater.* **2002**, *14*, 1625–1629; g) S. K. Samanta, A. Pal, S. Bhattacharya, *Langmuir* **2009**, *25*, 8567–8578; h) S. K. Samanta, A. Pal, S. Bhattacharya, C. N. R. Rao, *J. Mater. Chem.* **2010**, *20*, 6881–6890; i) S. J. George, T. F. A. de Greef, R. Bovee, J. L. J. van Dongen, A. P. H. J. Schenning, E. W. Meijer, *Chem. Asian J.* **2009**, *4*, 910–917; j) S. K. Samanta, S. Bhattacharya, *Chem. Eur. J.*, DOI: 10.1002/chem.201103855; k) S. K. Samanta, S. Bhattacharya, *J. Mater. Chem.*, DOI: 10.1039/c2jm35012b.

[6] a) J. S. Treger, V. Y. Ma, Y. Gao, C.-C. Wang, H.-L. Wang, M. S. Johal, *J. Phys. Chem. B* **2008**, *112*, 760–763; b) C. Zhu, Q. Yang, L. Liu, F. Lv, S. Li, G. Yang, S. Wang, *Adv. Mater.* **2011**, *23*, 4805–4810.

[7] a) Y. Tang, E. H. Hill, Z. Zhou, D. G. Evans, K. S. Schanze, D. G. Whitten, *Langmuir* **2011**, *27*, 4945–4955; b) Y. Wang, T. S. Corbitt, S. D. Jett, Y. Tang, K. S. Schanze, E. Y. Chi, D. G. Whitten, *Langmuir* **2012**, *28*, 65–70; c) Y. Wang, Y. Tang, Z. Zhou, E. Ji, G. P. Lopez, E. Y. Chi, K. S. Schanze, D. G. Whitten, *Langmuir* **2010**, *26*, 12509–12514; d) Y. Wang, T. D. Canady, Z. Zhou, Y. Tang, D. N. Price, D. G. Bear, E. Y. Chi, K. S. Schanze, D. G. Whitten, *ACS Appl. Mater. Interfaces* **2011**, *3*, 2209–2214.

[8] a) M. George, S. L. Snyder, P. Terech, C. J. Glinka, R. G. Weiss, *J. Am. Chem. Soc.* **2003**, *125*, 10275–10283; b) A. Pal, Y. K. Ghosh, S. Bhattacharya, *Tetrahedron* **2007**, *63*, 7334–7348; c) J. Cui, Y. Zheng, Z. Shen, X. Wan, *Langmuir* **2010**, *26*, 15508–15515.

[9] a) H. Kobayashi, A. Friggeri, K. Koumoto, M. Amaike, S. Shinkai, D. N. Reinhoudt, *Org. Lett.* **2002**, *4*, 1423–1426; b) A. Srivastava, S. Ghorai, A. Bhattacharjya, S. Bhattacharya, *J. Org. Chem.* **2005**, *70*, 6574–6582; c) Y. Qiao, Y. Lin, Z. Yang, H. Chen, S. Zhang, Y. Yan, J. Huang, *J. Phys. Chem. B* **2010**, *114*, 11725–11730.

[10] J. W. Chung, B.-K. An, S. Y. Park, *Chem. Mater.* **2008**, *20*, 6750–6755.

[11] S. Bhattacharya, A. Pal, *J. Phys. Chem. B* **2008**, *112*, 4918–4927.

[12] a) H. A. Barnes, *A Handbook of Elementary Rheology*, University of Wales, Institute of Non-Newtonian Fluid Mechanics, Aberystwyth, **2000**, pp. 55–61; b) F. M. Menger, K. L. Caran, *J. Am. Chem. Soc.* **2000**, *122*, 11679–11691; c) P. Terech, D. Pasquier, V. Bordas, C. Rossat, *Langmuir* **2000**, *16*, 4485–4494;d) A. Pal, H. Basit, S. Sen, V. K. Aswal, S. Bhattacharya, *J. Mater. Chem.* **2009**, *19*, 4325–4334.

[13] a) D. C. Duncan, D. G. Whitten, *Langmuir* **2000**, *16*, 6445–6452; b) J. H. Jung, S. Shinkai, T. Shimizu, *Chem. Eur. J.* **2002**, *8*, 2684–2690; c) D. K. Kumar, D. A. Jose, P. Dastidar, A. Das, *Langmuir* **2004**, *20*, 10413–10418; d) Y.-T. Shen, C.-H. Li, K.-C. Chang, S.-Y. Chin, H.-A. Lin, Y.-M. Liu, C.-Y. Hung, H.-F. Hsu, S.-S. Sun, *Langmuir* **2009**, *25*, 8714–8722.

[14] S. Yagai, S. Kubota, H. Saito, K. Unoike, T. Karatsu, A. Kitamura, A. Ajayaghosh, M. Kanesato, Y. Kikkawa, *J. Am. Chem. Soc.* **2009**, *131*, 5408–5410.

[15] H. Basit, A. Pal, S. Sen, S. Bhattacharya, *Chem. Eur. J.* **2008**, *14*, 6534–6545.

[16] a) S. K. Samanta, A. Gomathi, S. Bhattacharya, C. N. R. Rao, *Langmuir* **2010**, *26*, 12230–12236; b) S. K. Samanta, K. S. Subrahmanyam, S. Bhattacharya, C. N. R. Rao, *Chem. Eur. J.* **2012**, *18*, 2890–2901.

[17] a) B. Juskowiak, M. Ohba, M. Sato, S. Takenaka, M. Takagi, H. Kondo, *Bull. Chem. Soc. Jpn.* **1999**, *72*, 265–277; b) J. Tang, C. Wang, Y. Wang, J. Sunb, B. Yang, *J. Mater. Chem.* **2001**, *11*, 1370–1373; c) E. P. Petrov, F. Cichos, F. Wagner, St. Spange, C. von Borczyskowski, *Photochem. Photobiol.* **2005**, *81*, 898–907; d) C.-X. Yuan, X.-T. Tao, Y. Ren, Y. Li, J.-X. Yang, W.-T. Yu, L. Wang, M.-H. Jiang, *J. Phys. Chem. C* **2007**, *111*, 12811–12816.

[18] The excitation and emission maximum of the hydrogel of **2** appeared at 470 and 590 nm, respectively, when recorded under the front-face geometry. Therefore, the emission maximum at 600 nm in the case of addition of NaBr ensured aggregated emission (see Figure S6 in the Supporting Information).

[19] a) Y.-L. Liu, Y.-H. Wu, C.-Y. Hsu, *Nanotechnology* **2009**, *20*, 235704; b) X. Wang, J. Yan, Y. Zhou, J. Pei, *J. Am. Chem. Soc.* **2010**, *132*, 15872–15874; c) C. Vijayakumar, K. Sugiyasu, M. Takeuchi, *Chem. Sci.* **2011**, *2*, 291–294; d) C. Giansante, G. Raffy, C. Schafer, H. Rahma, M.-T. Kao, A. G. L. Olive, A. del Guerzo, *J. Am. Chem. Soc.* **2011**, *133*, 316–325; e) Y. Hong, J. W. Y. Lam, B. Z. Tang, *Chem. Soc. Rev.* **2011**, *40*, 5361–5388; f) M. R. Molla, S. Ghosh, *Chem. Eur. J.* **2012**, *18*, 1290–1294; g) A. Ajayaghosh, V. K. Praveen, C. Vijayakumar, S. J. George, *Angew. Chem.* **2007**, *119*, 6376–6381; *Angew. Chem. Int. Ed.* **2007**, *46*, 6260–6265; h) R. Abbel, R. van der Weegen, E. W. Meijer, A. P. H. J. Schenning, *Chem. Commun.* **2009**, 1697–1699; i) R. Abbel, R. van der Weegen, W. Pisula, M. Surin, P. Leclere, R. Lazzaroni, E. W. Meijer, A. P. H. J. Schenning, *Chem. Eur. J.* **2009**, *15*, 9737–9746.

[20] R. Varghese, S. J. George, A. Ajayaghosh, *Chem. Commun.* **2005**, 593–595.

[21] a) C. D. Geddes, *Meas. Sci. Technol.* **2001**, *12*, R53–R88; b) A. Chmyrov, T. Sanden, J. Widengren, *J. Phys. Chem. B* **2010**, *114*, 11282–11291.

[22] J. R. Lakowicz, in *Principles of Fluorescence Spectroscopy*, Springer, New York, **2006**, p. 11, 3rd ed.

[23] a) F. Hofmeister, *Arch. Exp. Pathol. Pharmakol.* **1888**, *24*, 247–260; b) Y. Zhang, P. S. Cremer, *Curr. Opin. Chem. Biol.* **2006**, *10*, 658–663; c) L. Xu, X. Li, M. Zhai, L. Huang, J. Peng, J. Li, G. Wei, *J. Phys. Chem. B* **2007**, *111*, 3391–3397; d) L. M. Pegram, M. T. Record, *J. Phys. Chem. B* **2008**, *112*, 9428–9436; e) J. M. G. Swann, W. Bras, P. D. Topham, J. R. Howse, A. J. Ryan, *Langmuir* **2010**, *26*, 10191–10197; f) H. Wang, Q. Feng, J. Wang, H. Zhang, *J. Phys. Chem. B* **2010**, *114*, 1380–1387; g) C. P. Schneider, D. Shukla, B. L. Trout, *J. Phys. Chem. B* **2011**, *115*, 7447–7458; h) Y. Zhang, P. S. Cremer, *Annu. Rev. Phys. Chem.* **2010**, *61*, 63–83; i) A. Klaus, G. J. T. Tiddy, R. Rachel, A. P. Trinh, E. Maurer, D. Touraud, W. Kunz, *Langmuir* **2011**, *27*, 4403–4411.

Received: June 1, 2012
Revised: August 31, 2012
Published online: November 23, 2012

